Mine Water and the Environment (2023) 42:251–265
https://doi.org/10.1007/s10230-023-00933-7

TECHNICAL ARTICLE

Experimental Study on the Mechanical Damage and Deformation Failure of Water-bearing Coal Samples

Qiangling Yao[1,2] · Liqiang Yu[1,2] · Changhao Shan[1,2] · Ze Xia[1,2] · Ning Chen[1,2] · Hongxin Xie[1,2] · Liu Zhu[1,2]

Received: 22 May 2022 / Accepted: 10 May 2023 / Published online: 27 May 2023

Abstract

The stability, design, and evaluation of coal-pillar dams are affected by how water and mining affect the mechanical performance and failure mode of coal. We analyzed the composition and water-absorption mechanisms of coal samples taken from the Chahasu coal mine in western China by x-ray diffraction and nondestructive water-soaking tests. Uniaxial compression tests were carried out on coal samples with different moisture contents and loading rates to investigate their mechanical properties and deformation damage characteristics while monitoring the acoustic emissions. The compressive strength and modulus of elasticity decreased with increased moisture content, with maximum attenuations of 50.3% and 42.4%, respectively. Increasing the loading rate caused the compressive strength and elastic modulus to first increase and then decrease; the maximum increases were 74.2% and 82.5%. With low moisture content and low loading rate, the coal samples become brittle; the main failure mode was tensile failure. Increasing the moisture content enhanced the plasticity of the coal samples, leading to more shear cracks and a switch in failure mode from tensile failure to shear failure. The increased loading rate reduces the effect of water on coal samples and increases the tensile effect. High loading rates tend to produce conical failure features. Acoustic emission characteristics were used as the basis for classifying the stress stages of coal samples, which further supplements the analysis of the failure process of coal samples. Finally, the reference of this study to field engineering practice and its own limitations were analyzed. These results should help guide the design of stable underground hydraulic systems and advance our understanding of rock-fracture-failure mechanisms in a water-rich environment.

Keywords Western China · Moisture content · Loading rate · Mechanical properties · Acoustic emission

Introduction

Fossil energy in the form of coal still accounts for most of the world's energy supply and for 58% of China's total energy consumption (British Petroleum 2019). In 2021, the output of raw coal from the five provinces of Shanxi, Shaanxi, Inner Mongolia, Xinjiang, and Ningxia amounted to about 3.34 billion tons, accounting for 82% of the country's total output (National Bureau of Statistics of the People's Republic of China 2021). However, the western region is in an arid and semi-arid zone with scarce water resources, and the supply of water resources in the area does not satisfy the demand. Newly developed water-preserving mining technology (Liu et al. 2018; Sun et al. 2018; Zhang et al. 2017) and goaf water-storage technology (Gu 2015; Gui et al. 2018; Li et al. 2018) have alleviated the water-resource problem for coal mining in these areas. After destroying the water-containing layer, the confined space (underground reservoir) in the goaf formed by the coal-pillar dam can contribute to protecting water resources (Tang 2019). In a water-rich environment, water degrades the mechanical strength of the coal-rock mass, which greatly affects the stability and impermeability of coal-pillar dams. Thus, the mechanical properties and failure modes of water-containing coal should be investigated to determine the proper size of coal-pillar dams and how to design adjacent structures that do not allow water seepage, both of which are important for the construction and safe operation of underground-reservoir projects in coal mines.

Soaking in water changes the mineral composition and microstructure of coal rock by decreasing the cohesion of

✉ Liqiang Yu
yuliqiangcumt@163.com

[1] State Key Laboratory of Coal Resources and Safe Mining (CUMT), China University of Mining & Technology, Xuzhou 221116, China

[2] School of Mines, China University of Mining & Technology, Xuzhou 221116, China

mineral particles, which degrades the mechanical characteristics of coal rock. Numerous studies have investigated the mechanical properties of water-containing coal-rock. For example, Yang et al. (2017) studied the mechanical properties of natural and forced water-soaked coal samples through single-axis and three-axis static-loading compression tests and found that forced water soaking increases the saturated moisture content of coal samples and decreases the compressive strength and cohesion. Chen et al. (2017) conducted a single-axis compression experiment to compare coal-rock composite samples that were dry with samples containing intrinsic and saturated moisture content and found that the dry coal-rock composite sample was mechanically the strongest, followed by the coal-rock composite with intrinsic moisture content, and finally by the saturated coal-rock composite.

Investigating how moisture content affects the mechanical properties of a coal-rock mass showed that an increase in moisture content decreases the elastic modulus, rigidity, compressive strength, tensile strength, and other physical parameters (Vergara and Triantafyllidis 2016; Zhou et al. 2016), whereas the degree of plasticity and softening increases (Hu et al. 2017). While repeating water soaking experiments to study water-resistant coal and rock pillars, Yao et al. (2011, 2015, 2016) developed a nondestructive experimental device for soaking, which they used to study how drying-saturation cycles affect the mechanisms of mechanical damage and the acoustic emission (AE) of coal and rock samples. Yilmaz et al. (2009) indicated that, in the Mohr–Coulomb failure criterion, in which the friction angle determines how rock strength is reduced by water, the deformation of water-containing sedimentary rock is greater than in the dry state and is manifested as an increase in Poisson's ratio and a decrease in Young's modulus.

Coal pillar dams are an important part of underground reservoirs and are affected not only by long-term exposure to water but also by subsidence stress in the strata overlying the goaf. Because of different mining intensities at adjacent workfaces, the loading rate of coal-pillar dams constantly changes due to the subsidence of overlying strata. The loading rate is thus an important engineering factor that varies over large scales and strongly affects the mechanical properties of coal and rock (Yang et al. 2005; Yin et al. 2010).

Currently, numerous laboratory tests have focused on brittle rocks. Other studies have considered how loading rates affect the strength of rocks such as fine sandstone, tuff, oil shale, limestone, and salt stone (Chong 1990; Lajtai 1991). Single-axis compression tests reveal that the compressive strength and elastic modulus of rock increase with loading rate (Li 1995; Martin 1993; Shams et al. 2015), whereas the bearing structure of coal samples tends to store more deformation energy under high loading rates (Li et al. 2016a, 2015). Li et al. (2016c) found that, as the loading rate increases, damage stress appears earlier in the coal sample and fails sooner, yet when the loading rate reaches the critical value, the load tends to stabilize. Li et al. (2016b) used numerical simulations to reveal that macroscopic damage decreases with an increased loading rate. As the loading rate increases, peak counts of AE and their energy increase, whereas accumulated counts of AE and their energy decrease. On the theory side, Alam et al. (2015) proposed an empirical equation that relates the dynamic increase to the applied strain rate. Qi et al. (2003) studied the strain-rate-dependent mechanism of brittle rock and deduced the strength-strain-rate-dependent model of brittle materials. These results and others have laid the foundation for the study of how loading rates affect the mechanical properties of rock.

To date, research into the effect of media-loading rate has focused mainly on brittle rock. However, the brittleness of coal is between that of hard rock and soft rock, and its mechanical response to loading rate differs from that of ordinary rock. In addition, the effect of water complicates the mechanics, and the relevant mechanisms causing internal damage in coal remain to be clarified. Thus, in this study, we first used x-ray diffraction (XRD) and nondestructive water-soaking experiments to deduce coal-sample composition and water-absorption mechanisms. Then, based on single-axis compression and AE experiments involving rocks with different moisture contents and loading rates, we investigated the characteristic mechanical damage and structural failure of coal samples. The results of this research should improve our fundamental understanding of the mechanisms of damage to water-containing coal as a function of loading rate and provide a useful reference for the stability design of coal-pillar dams.

Methods

Materials and Preparation

Samples of the representative coal seam were collected near the coal pillar dam from the Chahasu coal mine in the Dongsheng coalfield of the Shendong mining area, China (see Fig. 1). The original coal samples were processed into Φ 50 mm × 100 mm standard cylindrical samples, according to the experimental requirements of the International Society for Rock Mechanics Test Specification (Muralha et al. 2014) and the Petrophysics Mechanical Properties Test Regulations DZ/T0276.25-2015 (Ministry of Land and Resources of the PRC 2015). Four typical moisture contents and four typical loading rates were selected as variables to cross-test the coal samples, with each set of variable combinations containing three specimens. The coal samples were divided into 16 groups of three each, for a total of 48, and numbered

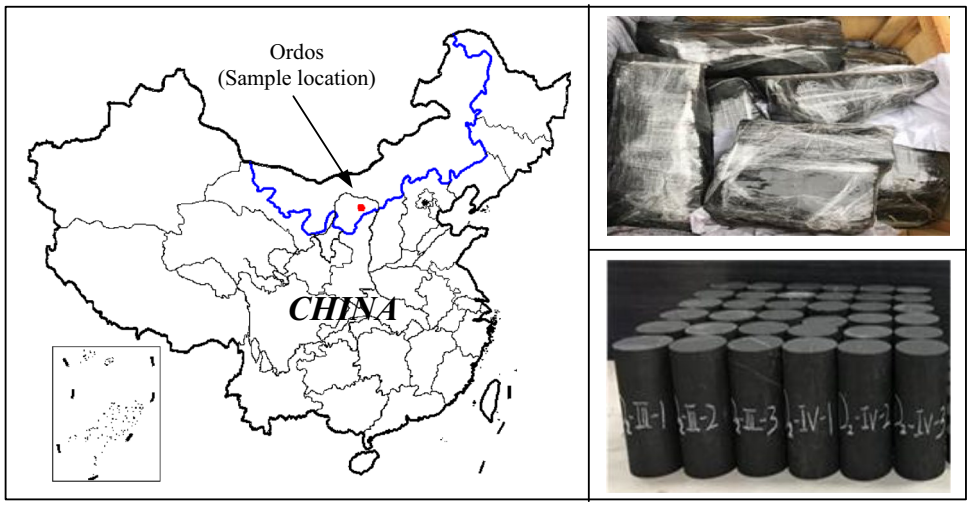

Fig. 1 Sampling information

according to moisture content and loading rate. In the numbering convention, W is the moisture content, V is the loading rate, and the number is the serial number (see Table 1).

Sample Compositions

The XRD test results of the coal samples are shown in Table S-1 and Fig. S-1. The coal samples contain quartz (12%), plagioclase (3%), calcite (4%), clay minerals (7%), and other minerals (74%); the clay minerals are mainly kaolinite (9%) and chlorite (91%). The quartz is a high-strength rock-forming mineral that increases the strength of coal samples. Carbonate minerals such as calcite can fill cracks in the coal and can remain relatively stable for long periods and have little effect on the coal sample. After soaking the coal samples in water, part of the free water intrudes into the clay minerals; the kaolinite in the clay has strong absorbability and plasticity after being exposed to water. Furthermore, chlorite thickens when it absorbs water, which increases the rock volume (Fang et al. 2018).

Instrumentation and Methods

An air-blowing drier (Type 101-2, Shanghai Instrument Factory, China) was used to dry the coal samples. As per the requirements of the petrophysical mechanical properties test procedure DZ/T 0276.2-2015 (Ministry of Land and Resources of the PRC 2015), the drying temperature was set to 105 °C, and the coal samples were dried for 12 h (h). At this point, the moisture content of the sample is 0% and the mass of the sample will no longer decrease with a longer drying time (Yao et al. 2019). A nondestructive water-soaking apparatus (Yu et al. 2020; Type HL-8-1WS, China University of Mining and Technology & Dongying Cortes Test Instrument Co., Ltd., China) was used to soak the coal samples in water. The atomiser was connected to the humidification space inside the device by built-in piping. The coal sample was exposed to the constant-humidity water vapor in the humidification space until it was saturated. The change in the quality of the coal sample was monitored in real time by the bottom sensor and plotted as a function of the moisture content by a signal converter (Yu et al. 2022). The coal samples freely absorbed water while in the saturated-humidity water vapor area at constant temperature and humidity. This avoided damaging the coal samples that can occur when they are directly soaked in water and thus ensured the integrity of the coal samples. The loading system used an electro-hydraulic servo universal testing machine (Type C64.106, MTS Systems Corp., USA) to do single-axis compression experiments on the coal samples at loading rates of 0.1, 0.2, 0.5, and 1.0 mm/min. The AE signals of the coal samples were monitored during compression using an AE monitoring system (Type PCI-II, American Physics Acoustic Co., USA). To accurately localize the AE source, four probes

Table 1 Meaning of sample number

Loading rate/moisture content	0%	2.32%	5.79%	9.37%
0.1 mm/min	W1-V1-1(2,3)	W2-V1-1(2,3)	W3-V1-1(2,3)	W4-V1-1(2,3)
0.2 mm/min	W1-V2-1(2,3)	W2-V2-1(2,3)	W3-V2-1(2,3)	W4-V2-1(2,3)
0.5 mm/min	W1-V3-1(2,3)	W2-V3-1(2,3)	W3-V3-1(2,3)	W4-V3-1(2,3)
1.0 mm/min	W1-V4-1(2,3)	W2-V4-1(2,3)	W3-V4-1(2,3)	W4-V4-1(2,3)

were arranged at the upper and lower 1/3 points on four sides of each cylinder. Figure 2 shows the test system.

Results and Discussion

The Water-Absorption Mechanism of the Coal Samples

Figure 3 plots the moisture content of the coal samples as a function of soaking time. Based on the water absorption speed of the coal samples, which is the slope of the curve, the curve can be divided into three stages: (i) fast growth, (ii) slow growth, and (iii) basic saturation. During the first 8 h that the initially dry coal samples were in contact with water, the coal surface quickly absorbed water, and the moisture content in the coal increased at a rapidly increasing rate. From 8 to 21 h, the water infiltrated from the surface into the bulk of the coal samples, gradually completing the water-absorption process. Although the moisture content increased in this stage, the water absorption rate decreased. Next, from 21 to 40 h, when the coal samples were close to saturated, the absorption rate approached zero, and the moisture content essentially remained unchanged. After 40 h, the moisture content of the saturated coal samples was 9.37%. Overall, the water-absorption capacity of the coal samples, which is related to the extensive distribution of internal pores and cracks, was satisfactory. The moisture content of the coal samples was related logarithmically to the soaking time as follows:

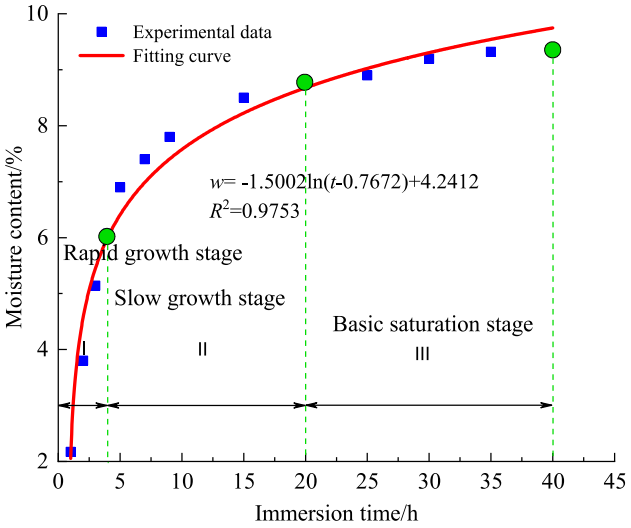

Fig. 3 Moisture content as a function of soaking time

$$W = -1.5002\ln(t - 0.7672) + 4.2412, R^2 = 0.9753 \quad (1)$$

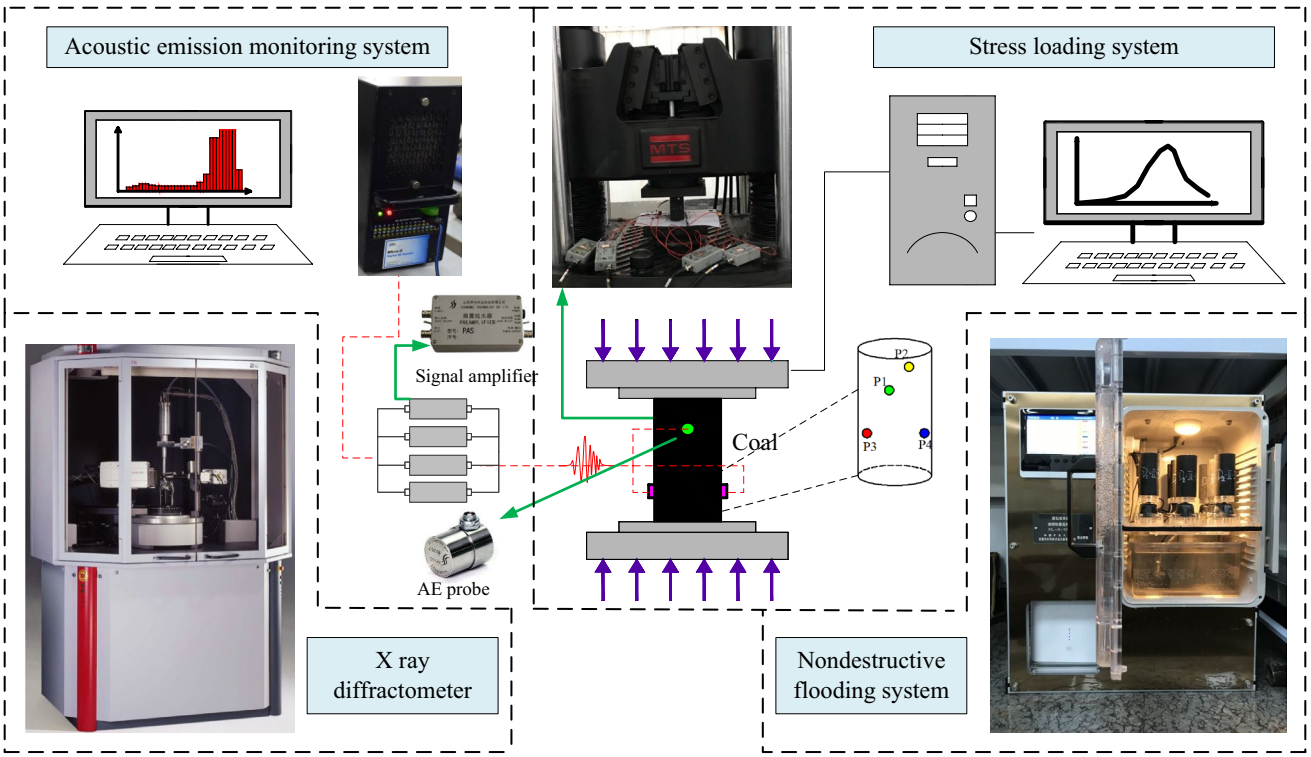

Fig. 2 Schematic showing the experimental system

where W is the moisture content (%), t is the soaking time (h), and R^2 is the correlation coefficient of the fitted curve. The result, $R^2 = 0.9753 \approx 1$, indicates a good fit. Herein, the characteristic moisture content (0%, 2.32%, 5.79%, and 9.37%) of the three water-absorption stages of the coal samples is regarded as a variable.

Mechanical Damage to the Coal Samples due to Moisture Content

Figure 4 and Table S-2 show the full stress–strain curves and mechanical properties of the coal samples with various moisture contents. To describe the crack-development mode in single-axis compression (Yu et al. 2020), the stress–strain curve of the coal can be divided into five stages: (i) crack compaction, (ii) elastic deformation, (iii) stable crack expansion, (iv) unstable crack expansion, and (v) unloading failure (Eberhardt et al. 1998; Hoke and Bienawski 1965). Compared with dry coal samples, the saturated coal samples were more prone to fluctuations in the stress–strain curve prior to the peak stress, which reflects the "stress mutation" phenomenon. This phenomenon is mostly concentrated near the peak stress at high loading rates. In the saturated state, the coal samples were greatly weakened, which substantially reduced their overall and local surface strength, which in turn facilitated local damage to the coal samples by small stresses, thereby causing stress mutation. Additionally, under high loading rates, the stress of the coal samples increased faster, and the stress-mutation phenomenon becomes more evident.

After the moisture content increased, the coal sample compaction curve became smoother due to the increased compressibility of the coal samples and the clay minerals after being softened by water. At the same time, the expansion of some clay minerals (e.g. chlorite) in contact with the

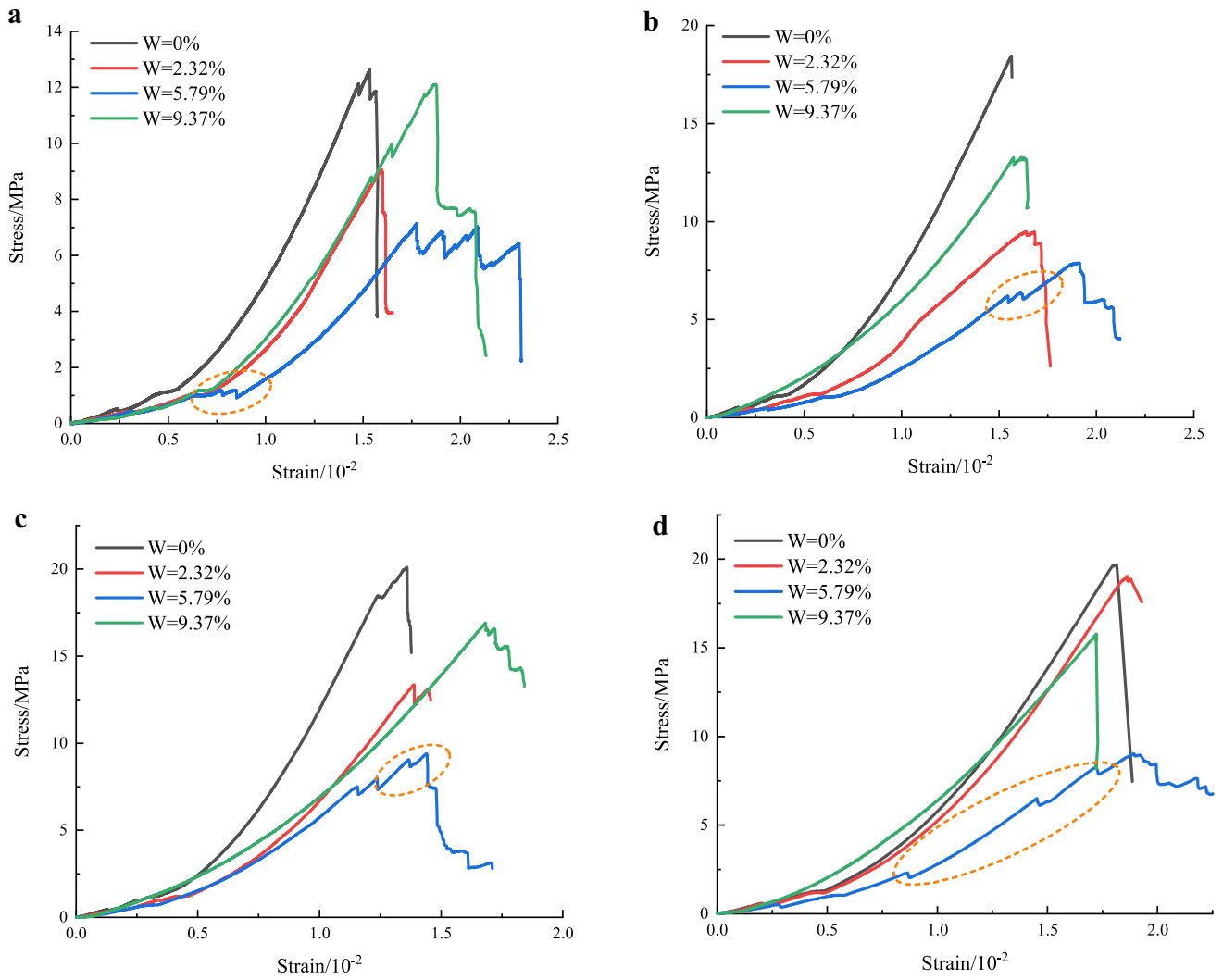

Fig. 4 Stress-strain curves of coal samples with different moisture contents. **a** V = 0.1 mm/min, **b** V = 0.2 mm/min, **c** V = 0.5 mm/min, **d** V = 1.0 mm/min

water also caused the expansion of primary cracks in the coal samples, which leads to prolonged compaction. Additionally, with increasing moisture content, the peak stress of the coal samples gradually decreases, while the peak strain continues to increase. The curve rises more smoothly in the elastic phase, and the coal samples demonstrated more plastic characteristics, which is consistent with previous research (Hu et al. 2017).

After the moisture content increased, the coal sample compaction curve became smoother due to the increased compressibility of the coal samples and the clay minerals after being softened by water. At the same time, the expansion of some clay minerals (e.g. chlorite) that were in contact with the water also caused the expansion of primary cracks in the coal samples, which led to prolonged compaction. Additionally, with increased moisture content, the peak stress of the coal samples gradually decreased, while the peak strain continued to increase. The curve rose more smoothly in the elastic phase, and the coal samples demonstrated more plastic characteristics, which is consistent with the results of previous research (Hu et al. 2017).

Figure 5 shows that the compressive strength of the coal samples decreased with increased moisture content. As an example, at a loading rate of 0.1 mm/min, the average compressive strength of the coal samples decreased from 12.8 to 12.0 MPa, 9.8Mpa, and 8.2Mpa, with an average attenuation of 6.3%, 23.4%, and 35.9%, respectively, as the moisture content increased from 0 to 9.37%. Overall, the coal samples at various loading rates tended to weaken when saturated, and to some extent, the compressive strength decreased more clearly at the high loading rates. During the water-coal interaction, water infiltrated into the coal samples and then reacted physically and chemically with the impurity minerals and cements therein. This reduced the cohesive force between coal particles and weakened the connection between particles (Cai 2002). Meanwhile, water enters the cracks and pores of the coal samples and generate hydrostatic pore pressure. Under the action of external compression, the pores expand, thereby leading to a decrease in the compressive strength of the coal samples (Wang et al. 2016).

Figure 6 plots the elastic modulus of the coal samples as a function of moisture content. The compressive strength of the coal samples decreased with increasing moisture content, but there was a decreasing trend in the rate of compressive strength's decrease. Under a loading rate of 0.1 mm/min, the average elastic modulus of the coal samples with 0% moisture content drops from 1109 Mpa to 892, 800, and 796 Mpa at moisture contents of approximately 2.32%, 5.79%, and 9.37%, for an average attenuation of 19.6%, 27.9%, and 28.2%, respectively. Likewise, at a loading rate of 0.5 mm/min, the average elastic modulus of coal samples with 0% moisture content dropped from 1798 MPa to 1627, 1213, and 1131 MPa at moisture contents of approximately 2.32%, 5.79%, and 9.37%, for an average attenuation of 9.5%, 32.5%, and 37.1%, respectively. Thus, the elastic modulus of water-containing coal is extremely sensitive to the loading rate. The influence of water on the elastic modulus of coal samples is related not only to the formation and structure of coal and the properties and composition of the solution (Eberhardt et al. 1998) but also to the mineral dissolution process and particle adhesion inside the coal samples. Once water enters the coal samples, it undergoes a hydrolysis reaction with the soluble substances in the cement and reduces the adhesive force between particles. Meanwhile, the lubricative effect of water also reduces the friction between particles, which is macroscopically expressed as a decrease in the

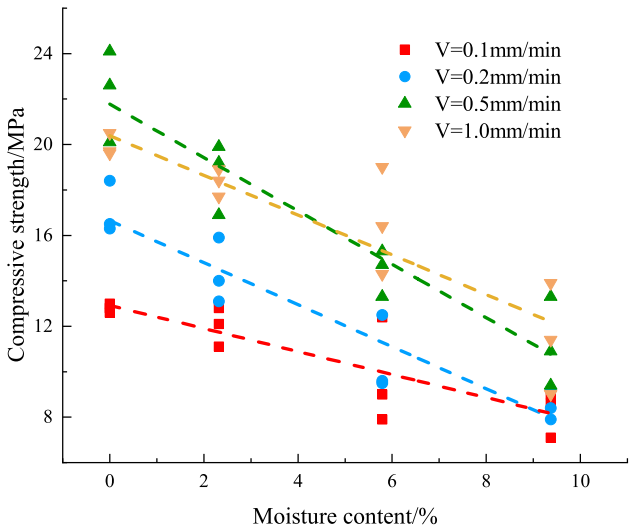

Fig. 5 Compressive strength of coal samples as a function of moisture content

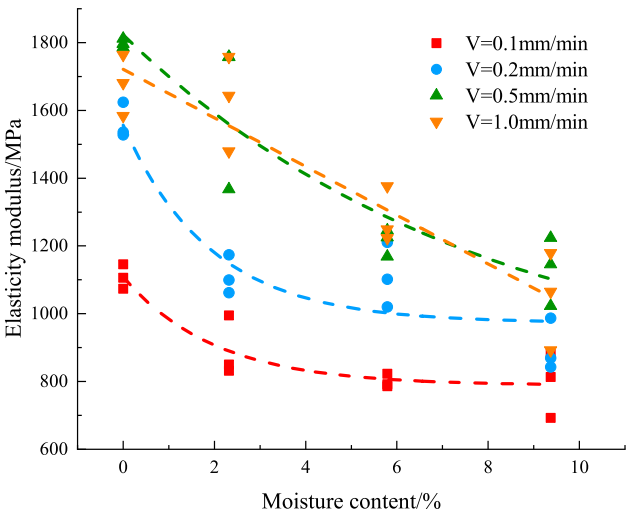

Fig. 6 Elastic modulus of coal samples as a function of moisture content relation

friction between the fracture surfaces and ultimately reduces the elastic modulus (Eberhardt et al. 1999) Under high loading rates, the stress in the coal samples rises relatively rapidly, the fracture surfaces are more prone to relative slip, and the elastic modulus decreases.

Mechanical Damage to Coal Samples due to Loading Rates

Figure 7 shows the full stress–strain curves of the coal samples with three moisture contents at different loading rates. The coal samples with low moisture content and high loading rates are brittle in the post-peak stage, and the stress drops quickly after the peak. This is because coal samples with low moisture content are not greatly weakened by being saturated with water, whereas the stress increases rapidly at high loading rates, and the internal energy accumulates quickly. After reaching peak stress, the energy was released very rapidly, which destroyed the coal sample. Additionally, compression of a coal sample at a low loading rate is slow, and the positive slope of the curve is near zero, reflecting the fact that the cracks in the coal sample were compressed and expanded fully at a low rate of stress growth. Although the coal samples rapidly compress under high loading rates, the positive slope of the curve was steeper. With an increased loading rate, the peak stress of the coal samples and the ultimate bearing capacity increased even further.

Figure 8 plots the compressive strength of the coal samples as a function of the loading rate. As the loading rate increased from 0.1 to 1.0 mm/min, the average compressive strength of the coal samples with 5.79% moisture content increased from 9.8 MPa to 10.5, 14.4, and 16.6 MPa at loading rates of 0.2, 0.5, and 1 mm/min, for an average increase of 7.1%, 43.8%, and 47.2%, respectively. Likewise, the compressive strength of the coal samples with 9.37% moisture content increases from 8.2 MPa to 8.5, 11.2, and 11.4 MPa,

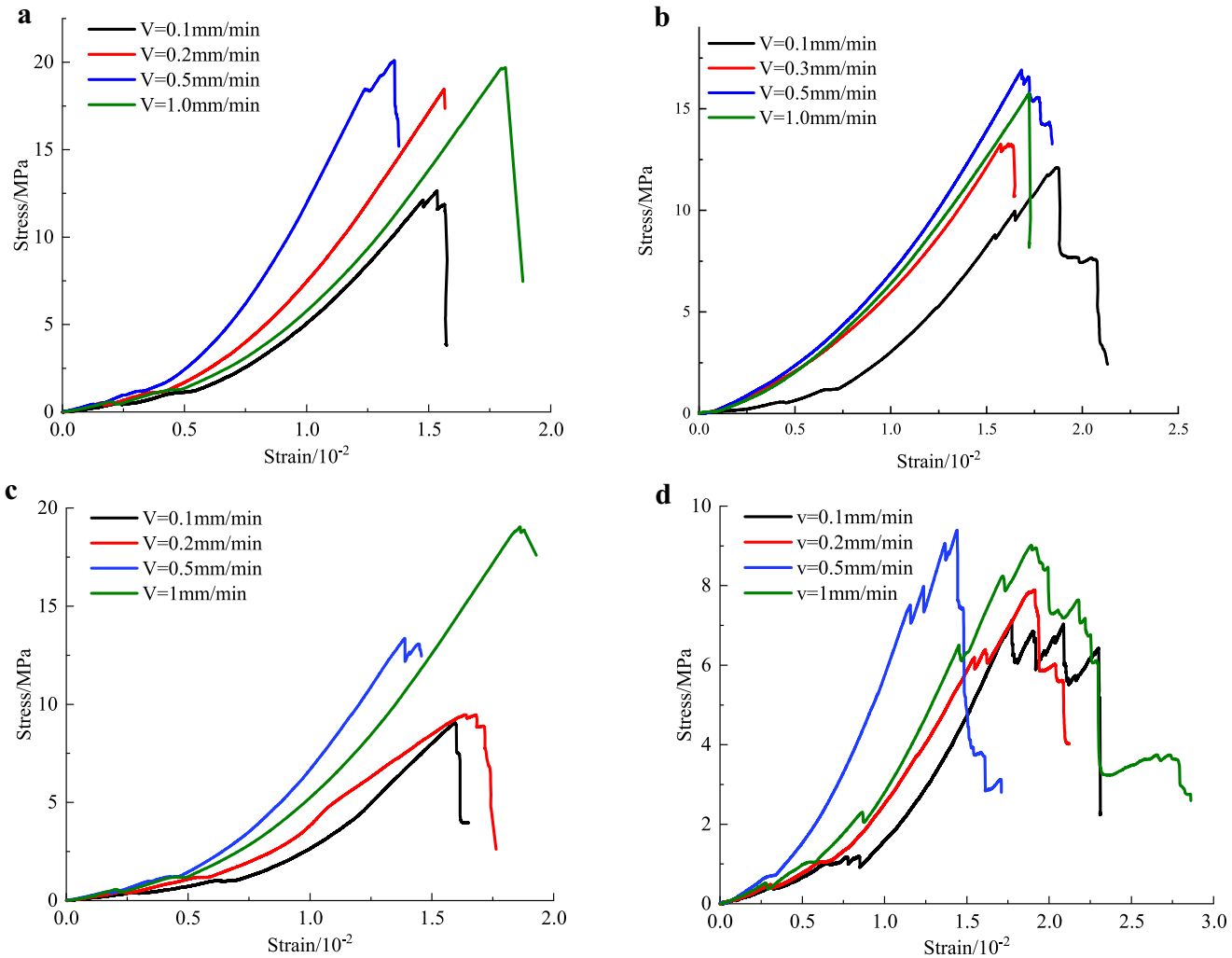

Fig. 7 Stress-strain curves of coal samples under various loading rates. **a** W = 0%, **b** W = 2.32%, **c** W = 5.79%, **d** W = 9.37%

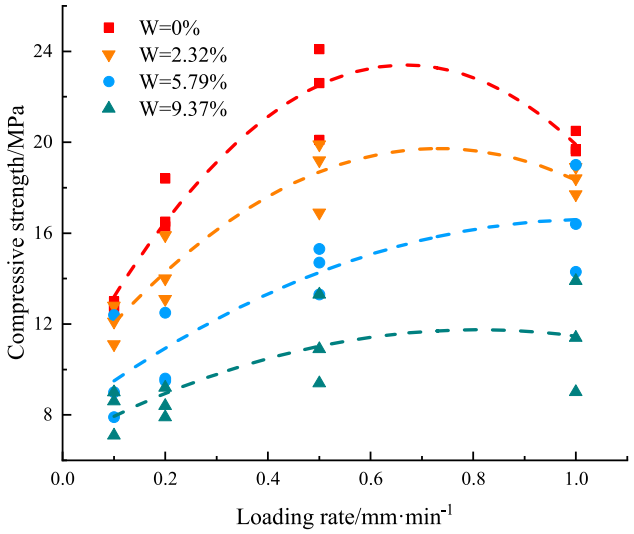

Fig. 8 Compressive strength as a function of loading rate

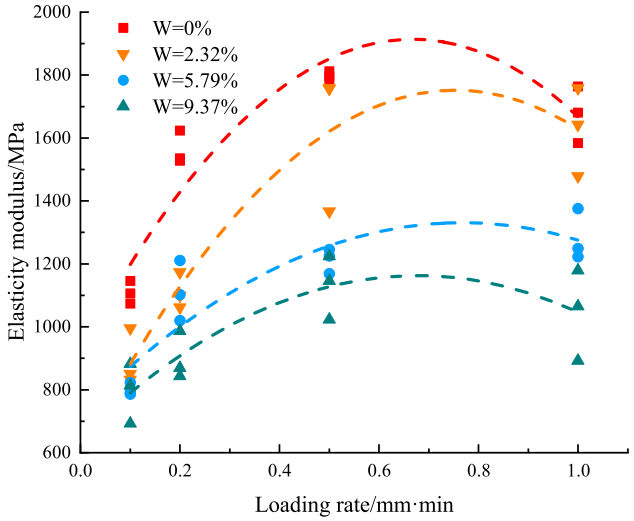

Fig. 9 Elastic modulus as a function of loading rate

at loading rates of 0.2, 0.5, and 1 mm/min, for an average increase of 3.4%, 36.6%, and 39.0%, respectively. To a certain extent, the compressive strength of the coal samples was positively correlated with the loading rate, which can be attributed to the fact that the growth in stress at low loading rates is slow, and the development of microstructure defects (such as primary cracks and secondary damage in the coal samples) and expansion is sufficient. This results in severe damage to the interior of the coal samples before reaching the peak stress, thereby reducing the load-bearing capacity of the coal samples. On the other hand, at high-loading rates, the internal-damage propagation time of the coal samples is limited, the crack activity is relatively suppressed, and the degree of accumulated damage in the early stage is reduced, resulting in high-strength characteristics on a macroscopic scale (Luo et al. 2018). It should be noted that when the coal samples are saturated (W = 9.37), the effect of water on their mechanical properties is greater, which in turn causes a small change in the correspondence between compressive strength and loading rate.

As the loading rate was increased incrementally, the compressive strength of the coal samples increased up to a critical value. For loading rates ranging from 0.1 to 0.5 mm/min, the compressive strength correlated positively with the loading rate. When the loading rate was increased to 1.0 mm/min, multiple sets of test data indicated that the compressive strength of the coal samples decreased compared with the previous loading rate, which differs from the general mechanical response of brittle rock to loading rate. Preliminary analyses indicate that the coal samples contain numerous cracks and that the coal was weaker than the brittle rock. After the loading rate rose to the critical value, the stress concentration of internal cracks in the coal samples was too high due to the excessively rapid stress growth rate, which facilitated sudden expansion and penetration, thereby reducing the load-bearing capacity. This was manifested in the experiments by severe damage to the coal samples. Additionally, the water and the loading rate affected the mechanical properties of pf coal is a mutually restrictive manner. At high moisture content, the compressive strength was less sensitive to the loading rate; the compressive strength of the moist coal samples changed only slightly as the loading rate rose.

Figure 9 shows the elastic modulus of the coal samples as a function of the loading rate. As an example, the coal samples with a moisture content of 5.79% increased from 800 MPa at a loading rate of ≈ 0.1 mm/min to 1111, 1213, and 1283 MPa at loading rates of ≈ 0.2, 0.5, and 1.0 mm/min, for an average increase of 38.9%, 51.6%, and 60.4%, respectively. As the loading rate increased, the elastic modulus of the coal samples tended to increase and then decrease, which was more evident at lower moisture contents. Like the compressive strength, the elastic modulus of the coal samples was affected by the loading rate and was not durative. In the range of 0.1–0.5 mm/min, the elastic modulus increased with the loading rate, and when the loading rate was in the range of 0.5–1.0 mm/min, the elastic modulus dropped after the peak. Thus, the critical value of the loading rate was between 0.5 and 1.0 mm/min.

Stress Threshold and Acoustic Emission Characteristics During the Failure Process

The destabilization damage of a coal sample consists of sequential stages of progressively increasing severity. Based on macroscopic deformation, the process of coal rock damage can be divided sequentially into the crack closure stage,

elastic deformation stage, stable crack growth stage, unstable crack growth stage, and post-peak stage. Although the full stress–strain curve reflects the overall stress and deformation pattern of a coal sample, it remains difficult to obtain a clear indication of the extent of damage within the sample. AEs, defined as an elastic wave propagating due to the rapid release of energy within a material (Lockner 1993), has been widely used in nondestructive testing and damage assessment (Aggelis 2011; Ohno and Ohtsu 2010) and can be used as a basis for classifying the stress stage of coal samples. Figure 10 shows the correspondence between AE counts, AE cumulative counts, and stress.

As shown in Fig. 10, the OA section is the crack closure stage, where the primary cracks within the coal sample gradually close, and the AE events are mainly caused by crack compression and friction. It should be noted that the letter "O" represents the coordinate origin. During this stage, the AE counts are low, and the cumulative AE counts grow steadily. The AB section is the elastic deformation stage, where the coal sample undergoes recoverable elastic deformation under axial stress, and the AE counts increase slightly compared with the previous stage. The BC section is the stage of stable crack growth where the sample develops irrecoverable deformation. New cracks begin to sprout and develop within the coal sample, AE counts increase, and the slope of the cumulative AE count curve increases. The CD section is the stage of unstable crack growth, where the degree of damage is most intense before the peak stress. As new cracks begin to penetrate and form larger cracks within the sample, the bearing structure of the sample gradually destabilizes, and AE counts begin to peak, with the cumulative AE count curve rising approximately vertically. Point D is the peak stress point of the coal sample, after which the sample enters the post-peak stage. The macroscopic damage that occurs in the coal sample releases a large amount of energy, with intense peaks in the AE counts and a peak in the cumulative AE count curve.

Numerous AE events in the dry coal samples occur mainly during the unstable crack growth stage and near the peak point, whereas almost no large-scale AE events occur during the crack closure stage and the elastic stage. The reason for this is that the high strength and stiffness of a dry coal sample makes the overall structure more stable and allows enough energy to be built up to resist external forces, whereas reaching the peak stress instantly releases a large amount of energy and causes complete destruction. As the moisture content increases, the distribution of AE events appears to change quite a bit. For example, a coal sample with a moisture content of 5.79% has fewer peak AE counts, and cumulative AE counts peak near the stress peak decreases a lot relative to the dry coal sample, although there are few AE events in the crack closure stage and elastic stage of the coal sample. Water weakens the cementation between the particles within the sample, reducing the strength and stiffness of the sample and preventing it from accumulating much energy, and the destruction of the sample gives it a more plastic character. Notably, the frequency of AE events increases for coal samples with a moisture content of 9.37%, and the number of AE events in the crack closure stage and elastic deformation stage increases greatly, with multiple AE count peaks. This means that more structural damage occurred in the early stages of the compression process, creating numerous microfractures in the coal sample. On the one hand, this is related to a degradation of the mechanical properties and an enhancement of the plastic characteristics of the coal sample due to the influence of water; on the other hand, the inhomogeneity of the sample itself and the distribution of internal primary pores and cracks can also affect the results.

Figure 10d shows the crack closure threshold, the crack growth threshold, the crack damage threshold, and the macroscopic damage threshold (corresponding to points A, B, C, and D, in Fig. 10) as a function of moisture content. The macroscopic damage threshold, as well as the crack damage threshold, decreases approximately linearly with increasing moisture content. Clearly, this is due to the softening and scouring effect of water, which weakens the mechanical properties of the coal sample and compromises the integrity of its load-bearing structure. Note that the crack growth threshold varies less with increasing moisture content, whereas the crack closure threshold remains almost constant or even increases slightly ($\sigma_{w=0\%} = 1.1515$ MPa, $\sigma_{w=5.79\%} = 1.1566$ MPa, $\sigma_{w=9.37\%} = 1.1617$ MPa). This result is attributed to a combination of two factors: the softening of the coal samples caused by the water facilitates fracture closure, and; crack closure requires higher stresses in water-bearing coal samples to overcome the pore water pressure. The two factors work against each other, resulting in a phenomenon where the moisture content has less influence on the structural changes of the coal sample during the initial period of loading.

Different types of cracks produce different AE waveforms during their generation and extension and the risetime/amplitude (RA) and average frequency (AF) values in AE are evidence of the type of internal cracks in the material. Risetime is a parameter of acoustic emission that represents the time elapsed between the first crossing of the threshold and the maximum amplitude of the signal. Low AF and high RA values represent shear cracks, and high AF and low RA values represent tension cracks (Arash et al. 2014). Based on the mathematical concept of the random data probability density function, the Matlab software functions *null* and *hist* were used to calculate the probability distribution density of the RA and AF values, and the results were fitted to a cloud plot, allowing for visual analysis of crack types. Figure 11 shows the distribution characteristics of RA-AF values for

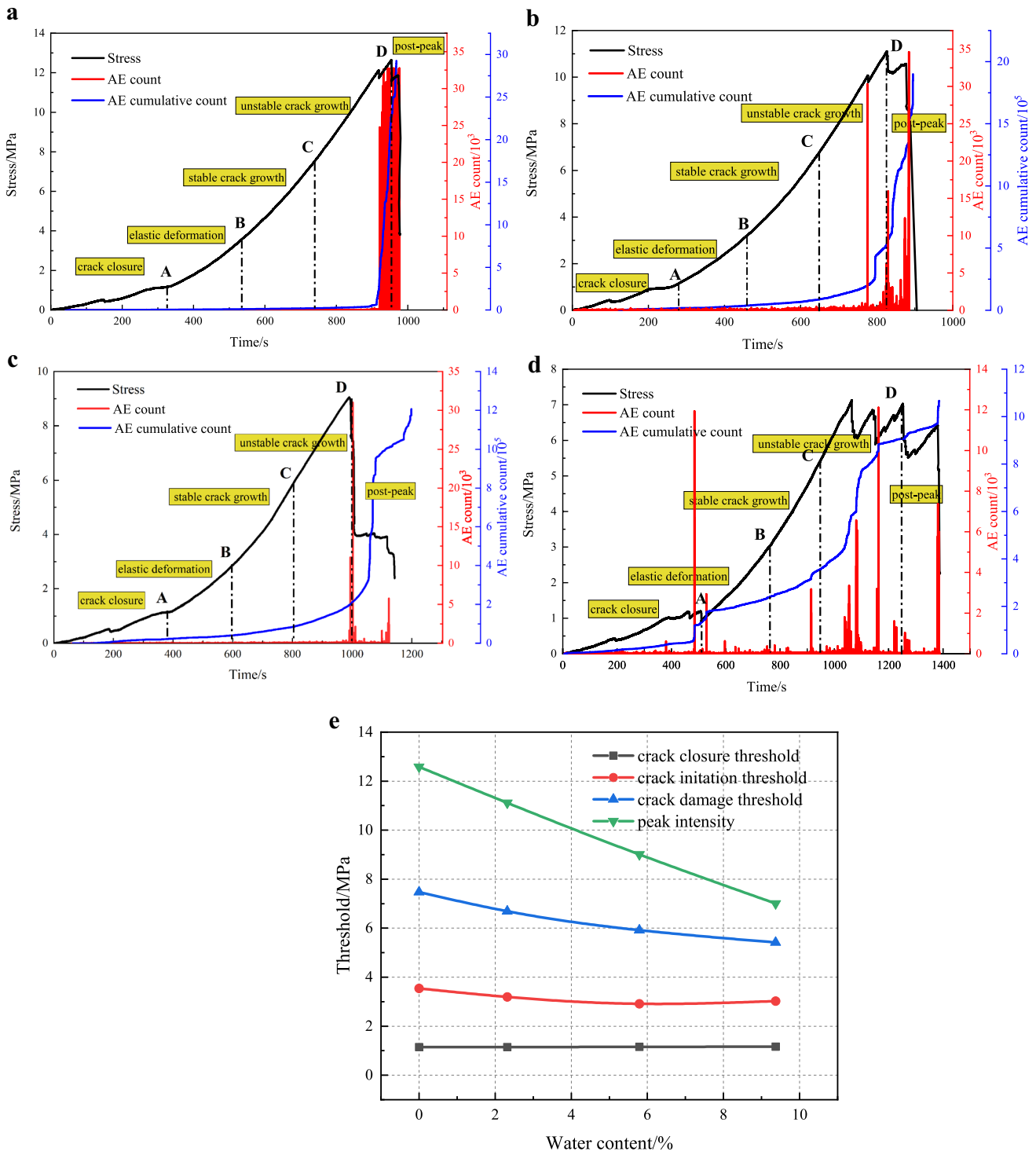

Fig. 10 AE count, cumulative count, and stress as a function of time and stress threshold as a function of moisture content for coal samples with different moisture contents. **a** W = 0%, **b** W = 2.32%, **c** W = 5.79%, **d** W = 9.37%, **e** stress threshold

coal samples with different moisture contents. The percent of high-density pixels (orange) in both tensile–shear (T–S) regions indicates that the coal samples with different moisture contents have an overall high AF value and low RA value (i.e. tensile cracks dominate the compression process in the coal samples). According to the Griffiths strength criterion, crack extension is caused by stress concentration near the crack tip, and rock-like materials generally have

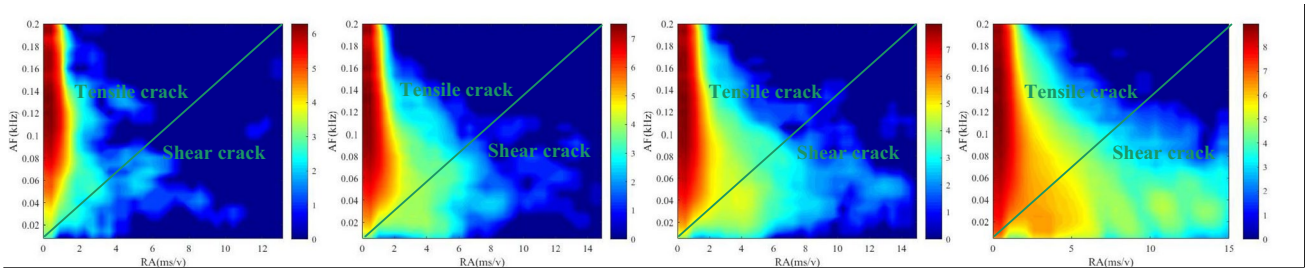

Fig. 11 RA-AF probability density distribution diagram of coal samples with different moisture content. **a** W = 0%, **b** W = 2.32%, **c** W = 5.79%, **d** W = 9.37%

less tensile strength than compressive strength, making them more susceptible to tensile cracking during compression. As the moisture content increased, the percent of high-density pixels in the T–S region changes. The high-density region gradually shifted to the lower right, which means that tensile cracks gradually decreased in number and shear cracks gradually increased in number. Furthermore, the increase in shear cracks also predicts a trend in the overall form of damage to the coal sample, which is analyzed in the next section.

Structural Failure of Coal Samples

The damage and failure modes of the coal samples involve the initiation, expansion, and penetration of internal cracks (Li et al. 2001). During single-axis compression, the failure modes of the coal samples can be summarized as x-shaped conjugate slope shear failure, single slope shear failure, and tensile failure, as shown in Fig. S-2. The study of the difference in the failure characteristics of the dynamically loaded, water-containing coal samples can provide a useful reference for exploring coal damage modes. Figure 12 shows the macro-failure characteristics of the coal samples in this experiment.

Figure 12 shows that the dry coal samples mainly generated tensile failure at low loading rates, and multiple axial cracks (see, e.g. W1-V1-1) appeared on the surface, which is related to the tensile strength of the coal-rock mass generally being less than the compressive strength (Niu 2017). The Poisson effect is active during the single-axis compression process of the coal samples, which affects the axial loading and constraints, and the horizontal tensile stress generated by the coal samples first reaches the strength limit and then fails, finally forming the axial tensile failure surface. When the coal samples are soaked in water, their moisture content increases, and water reduces the cohesive force and friction coefficient between mineral particles, facilitating local slippage between the surfaces of the coal samples under the action of small stresses, thereby leading to shear failure. With increased moisture, the probability of shear failure increases, especially at low loading rates (see, e.g. W1 ~ 4-V1-1 and W1 ~ 4-V2-1). The difference in moisture content also affects the failure of the coal samples. The dry coal samples are the most damaged, with the fragments being of small size and the copious powder particles having sharp edges and corners, with poor integrity after crushing. Again, a clear cracking sound is emitted during loading. With increased moisture content, the coal samples became more plastic, the degree of damage decreased, and the fragment size increased, although the coal samples remain relatively cylindrical after crushing.

Compared with the moisture content, the loading rate has a greater impact on the coal sample failure characteristics. At low loading rates, the failure modes of coal samples, especially tensile failures, are mainly determined by the moisture content. With increasing loading rate, the influence of water on the coal samples gradually diminishes. Since the tensile strength of the coal samples is less than the compressive strength, the tensile effect under high loading rates is more evident (see, e.g. W1-V1 ~ 4–1), whereas the coal samples that undergo shear failure will actually be subjected to multiple combined stresses, as manifested in the cone-shaped morphology of macroscopic failure (see, e.g. W3-V4-1). This is attributed to the fact that the shear stress dominates during the loading process and after the coal samples generate local weak surfaces. However, given the high loading rates, the stronger effect of shear stress is not obvious, so it changes to a combined action of simultaneous shear and tension. The coal sample failure morphology eventually becomes characterized by cones.

Moreover, the loading rate also affects the failure mode of the coal samples. Under low loading rates, the failure process of the coal samples is slow with low damage, and a larger volume of the remaining coal samples can be maintained. With an increased loading rate, the rapid increase in stress means that the coal samples quickly accumulate a great amount of energy. The failure process is thus rapid and causes a high degree of damage. Loud cracking sounds are emitted, and fragments of coal are ejected during the failure, making it difficult to retain complete coal samples.

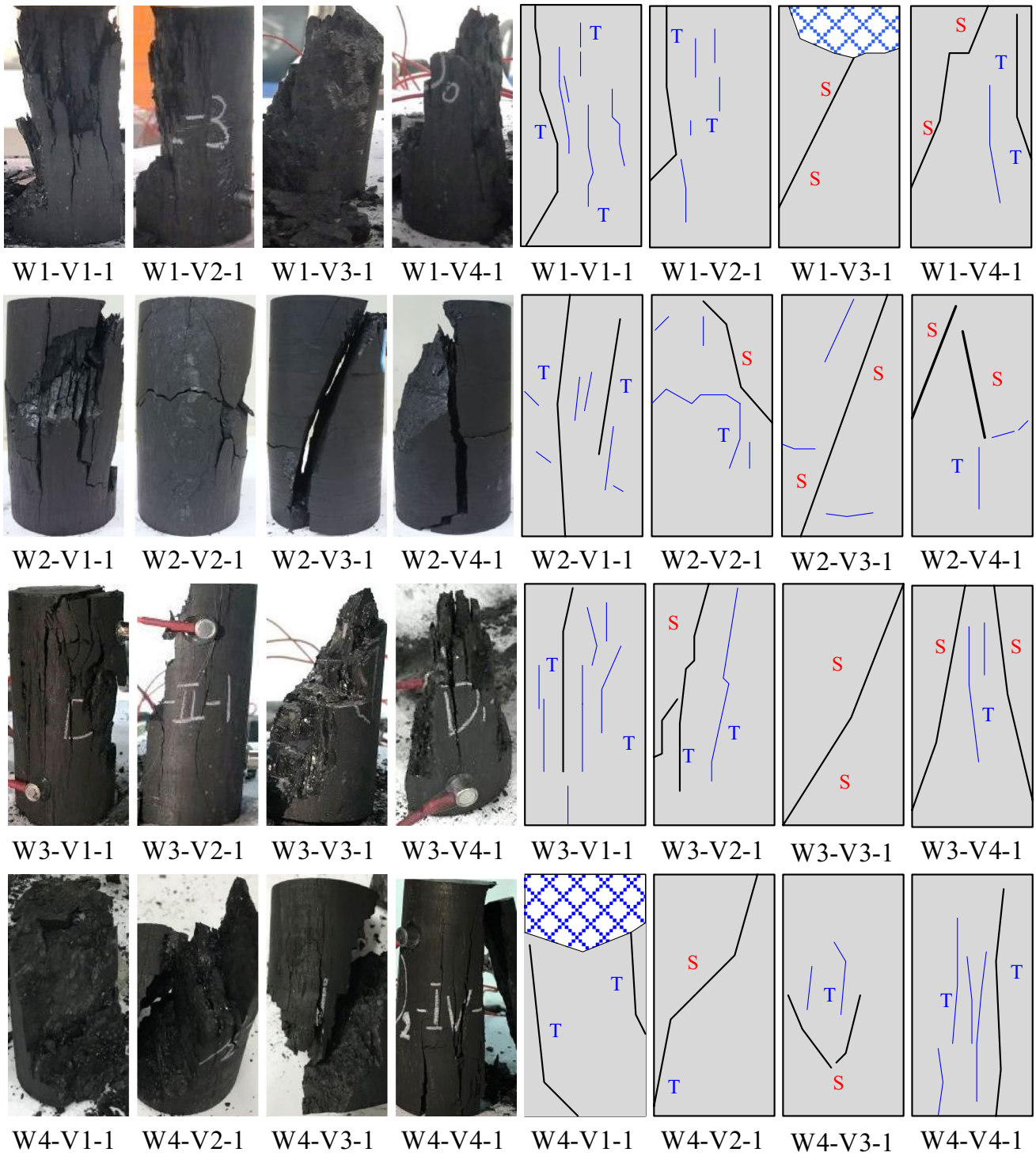

Fig. 12 Compression-failure characteristics of coal samples

Conclusions

In this study, a series of tests, including XRD, nondestructive water-soaking, AE monitoring, and uniaxial compression, were carried out on coal samples with different moisture contents and loading rates to investigate the mechanical properties and deformation damage characteristics. The main conclusions of this study were that:

The coal-sample moisture content was approximately logarithmic to the time exposed to the water vapor.

According to the slope of the curve, the moisture content can be divided into three stages: rapid growth (0–8 h), slow growth (8–21 h), and basic saturation (21–40 h). The subsequent tests were thus set at 0, 8, and 40 h, respectively, and the moisture contents were 0.00%, 5.79%, and 9.37%, respectively.

The mechanical performance of the coal samples depended on the moisture content and the loading rate. The compressive strength and elastic modulus of the coal samples decreased with respect to the moisture content, while to a certain extent, the compressive strength and elastic modulus of the coal samples were positively correlated with the loading rate. However, the strengthening effect of the loading rate was not durative but had a critical value. Therefore, with an increasing loading rate, the mechanical performance of the coal samples tended to first increase and then decrease.

Thus, the moisture content and loading rate affect the stress–strain curves of the coal samples. Coal samples with low moisture contents and low loading rates were brittle. With increased moisture content, the slope of the stress–strain curve decreased, and the plasticity increased. Water-saturated coal samples were prone to stress mutation before reaching the stress peak, and the mutations were mostly concentrated near the peak at high loading rates.

Dry coal samples easily undergo tensile failure; increasing the moisture content transforms the damage to shear failure, with a greater number of shear fractures and a reduced degree of damage. Yet the effects of the loading rate and moisture content on the failure mode of the coal samples are mutually restricted. Increasing the loading rate reduces the influence of the water on the coal samples. The effect of tension is more obvious, and the coal samples are more prone to cone-shaped failure at high loading rates.

As an essential component of underground reservoir in coal mine, the coal pillar dam is subjected to long-term exposure to water, which reduces its strength and poses a severe safety hazard. However, the strength variation of the coal pillar dam body becomes even more complex when coal mining activities are carried out at the working face adjacent to the coal pillar dam. Due to the varying intensity of mining activities, the rate of loading on the coal pillar dam from the subsidence of overlying strata in goaf continuously changes. This also affects the stability of the coal pillar dam. In this paper, the mechanical properties and deformation damage of coal samples under the influence of moisture content and loading rate were investigated by uniaxial compression experiments under AE monitoring. The results of this study provided basic mechanical parameters for the construction design of engineering rock masses under similar conditions and served as a reference for the subsequent stability assessment of engineering rock masses. Meanwhile, the RA-AF distribution cloud maps of the coal samples drawn based on AE data under different conditions can accurately and intuitively reveal the fracture development and damage patterns of coal samples, providing an effective method for the subsequent study of water-coal interaction. However, water-coal interaction is a complex process involving physical, chemical, and mechanical changes. The purified water used in this study met the general conditions but ignored some special cases where the mine water is acidic or alkaline due to solute transport and ion exchange. Further experimental and numerical simulations should be carried out to investigate how different conditions affect the mechanical properties and deformation damage of coal.

Supplementary Information The online version contains supplementary material available at https://doi.org/10.1007/s10230-023-00933-7.

Acknowledgements This research was funded by the National Natural Science Foundation of China (grant 51674248). The authors gratefully thank the reviewers for their constructive comments.

Data availability The data that support the findings of this study are available from the corresponding author upon reasonable request.

References

Aggelis DG (2011) Classification of cracking mode in concrete by acoustic emission parameters. Mech Res Commun 38(3):153–157. https://doi.org/10.1016/j.mechrescom.2011.03.007

Alam MS, Chakraborty T, Matsagar V, Rao KS, Sharma P, Singh M (2015) Characterization of Kota sandstone under different strain rates in uniaxial loading. Geotech Geol Eng 33(1):143–152. https://doi.org/10.1007/s10706-014-9810-3

Arash B, Hwa KC, Tomoki S (2014) Advanced structural health monitoring of concrete structures with the aid of acoustic emission. Constr Build Mater 65:282–302. https://doi.org/10.1016/j.conbuildmat.2014.04.103

BP statistical review of world energy 2019 Presentation (2019). British Petroleum, London, England. https://www.bp.com/en/global/corporate/paper-copies.html

Cai MF (2002) Rock mechanics and engineering. Science Press, Beijing

Chen T, Yao QL, Wei F, Chong ZH, Zhou J, Wang CB, Li J (2017) Effects of water intrusion and loading rate on mechanical properties of and crack propagation in coal–rock combinations. J Cent South Univ 24(2):423–431. https://doi.org/10.1007/s11771-017-3444-6

Chong KP, Boresi AP (1990) Strain rate dependent mechanical properties of New Albany reference shale. Int J Rock Mech Min Sci Geomech Abstr 27(3):199–205. https://doi.org/10.1016/0148-9062(90)94328-Q

Eberhardt E, Stead D, Stimpson B, Read RS (1998) Identifying crack initiation and propagation thresholds in brittle rock. Can Geotech J 35:222–233. https://doi.org/10.1139/cgj-35-2-222

Eberhardt E, Stimpson B, Stead D (1999) Effects of grain size on the initiation and propagation thresholds of stress-induced brittle fractures. Rock Mech Rock Eng 32(2):81–99. https://doi.org/10.1007/s006030050026

Fang J, Yao QL, Wang WN, Tang CJ, Wang G (2018) Experimental study on damage characteristics of siltstone under water action. J China Coal Soc 43(S2):412–419. https://doi.org/10.13225/j.cnki.jccs.2018.0629

Gu DZ (2015) Theory framework and technological system of coal mine underground reservoir. J China Coal Soc 40(2):239–246. https://doi.org/10.13225/j.cnki.jccs.2014.1661

Gui HR, Qiu HL, Qiu WZ, Tong S, Zhang H (2018) Overview of goaf water hazards control in China coalmines. Arab J Geosci 11(3):49. https://doi.org/10.1007/s12517-018-3391-z

Hoek E, Bienawski ZT (1965) Brittle fracture propagation in rock under compression. Int J Fract Mech 1:137–155. https://doi.org/10.1007/BF00186851

Hu KF, Feng Q, Wang XT (2017) Experimental research on mechanical property of phyllite tunnel surrounding rock under different moisture state. Geotech Geol Eng 35(1):303–311. https://doi.org/10.1007/s10706-016-0107-6

Lajtai EZ, Duncan EJS, Carter BJ (1991) The effect of strain rate on rock strength. Rock Mech Rock Eng 24(2):99–109. https://doi.org/10.1007/BF01032501

Li YS (1995) Experimental study on mechanical effect of loading rate on red sandstone. J Tongji Univ 23(3):265–269

Li HB, Zhao J, Li YJ (2001) The application of sliding crack model in the study of dynamic uniaxial compressive strength of rock. Chin J Rock Mech Eng 19(3):315–319

Li HT, Jiang CX, Jiang YD, Wang HW, Liu HB (2015) Mechanical behavior and mechanism analysis of coal samples based on loading rate effect. J Chin U Min Tech 44(3):430–436. https://doi.org/10.13247/j.cnki.jcumt.000326

Li HT, Song L, Zhou HW (2016a) Experimental study of nonlinear evolution mechanism of coal strength under multi-loading rates and its application. Chin J Rock Mech Eng 35(S1):2978–2989

Li XJ, Li HG, Yuan RF (2016b) Numerical simulation study of influence of loading rate on damage and acoustic emission characteristics of coal rock. J Henan Poly Univ Nat Sci 35(6):765–770. https://doi.org/10.16186/j.cnki.1673-9787.2016.06.003

Li YW, Jiang YD, Yang YM, Zhang KX, Ren Z, Li HT, Ma ZQ (2016c) Research on loading rate effect of uniaxial compressive strength of coal. J Min Safe Eng 33(4):754–760. https://doi.org/10.13545/j.cnki.jmse.2016.04.028

Li P, Ma LQ, Wu Y, Zhang L, Hao Y (2018) Concurrent mining during construction and water-filling of a goaf groundwater reservoir in a coal mine. Mine Water Environ 37(4):763–773. https://doi.org/10.1007/s10230-018-0537-x

Liu SL, Li WP, Wang QQ, He J, Xue S (2018) Water inrush risk zoning and water conservation mining technology in the Shennan mining area, Shaanxi China. Arab J Sci Eng 44(1):321–333. https://doi.org/10.1007/s13369-017-2858-7

Lockner DA (1993) The role of acoustic emission in the study of rock fracture. Int J Rock Mech Min Sci Geomech Abstr 30(7):883–899. https://doi.org/10.1016/0148-9062(93)90041-B

Luo K, Zhao GD, Zeng JJ, Zhang XX, Pu CZ (2018) Fracture experiments and numerical simulation of cracked body in rock-like materials affected by loading rate. Chin J Rock Mech Eng 37(8):62–71. https://doi.org/10.13722/j.cnki.jrme.2018.0080

Martin CD (1993) The strength of massive Lac du Bonner granite around underground openings. PhD Diss, Univ of Manitoba

Ministry of Land and Resources of the PRC (2015) Regulation for testing the physical and mechanical properties of rock. China Standard Press, Beijing **(in Chinese)**

Muralha J, Grasselli G, Tatone B, Blumel M, Chryssanthakis P, Yujing J (2014) ISRM suggested method for laboratory determination of the shear strength of rock joints: revised version. Rock Mech Rock Eng 47(1):291–302. https://doi.org/10.1007/s00603-013-0519-z

National Bureau of Statistics of the PRC (2021) Energy production in December 2021.https://baijiahao.baidu.com/s?id=1722169540468658316&wfr=spider&for=pc

Niu QH (2017) Experimental study on shear-damage law of water-bearing coal samples. PhD Diss, China Univ of Mining and Technology **(in Chinese)**

Ohno K, Ohtsu M (2010) Crack classification in concrete based on acoustic emission. Constr Build Mater 24(12):2339–2346. https://doi.org/10.1016/j.conbuildmat.2010.05.004

Qi WZ, Qian QH (2003) Physical mechanism of dependence of material strength on strain rate for rock-like material. Chin J Rock Mech Eng 22(2):177–181. https://doi.org/10.1142/S0252959903000104

Shams AM, Tanusree C, Vasant M, Seshagiri RK, Prince S, Manjit S (2015) Characterization of kota sandstone under different strain rates in uniaxial loading. Geotech Geol Eng 33(1):143–152. https://doi.org/10.1007/s10706-014-9810-3

Sun Q, Zhang JX, Zhou N, Qi W (2018) Roadway backfill coal mining to preserve surface water in western China. Mine Water Environ 37(2):366–375. https://doi.org/10.1007/s10230-017-0466-0

Tang CJ, Yao QL, Li ZY, Zhang Y, Ju MH (2019) Experimental study of shear failure and crack propagation in water-bearing coal samples. Energy Sci Eng 7(5):2193–2204. https://doi.org/10.1002/ese3.424

Vergara MR, Triantafyllidis T (2016) Influence of moisture content on the mechanical properties of an argillaceous swelling rock. Rock Mech Rock Eng 49(7):2555–2568. https://doi.org/10.1007/s00603-016-0938-8

Wang HL, Xu WY, Jia CJ, Cai M, Meng QX (2016) Experimental research on permeability evolution with microcrack development in sandstone under different fluid pressures. J Geotech Geoenviron 142(6):04016014. https://doi.org/10.1061/(ASCE)GT.1943-5606.0001462

Yang SJ, Zeng S, Wang HL (2005) Experimental analysis on mechanical effects of loading rates on limestone. Chin J Geotech Eng 26(7):786–788. https://doi.org/10.1007/s11769-005-0030-x

Yang WJ, Wang W, Li DY, Wang J, Liu WC (2017) Experimental study on mechanical characteristics of coal samples in natural and forced saturation state. J Safe Sci Technol 13(11):129–134

Yao QL (2011) Researches on strength weakening mechanism and control of water-enriched roofs of roadway. PhD Diss, China Univ of Mining and Technology **(in Chinese)**

Yao QL, Li XH, Zhou J, Ju MH, Chong ZH, Zhao B (2015) Experimental study of strength characteristics of coal samples after water intrusion. Arab J Geosci 8(9):6779–6789. https://doi.org/10.1007/s12517-014-1764-5

Yao QL, Chen T, Ju MH, Liang S, Liu Y, Li XH (2016) Effects of water intrusion on mechanical properties of and crack propagation in coal. Rock Mech Rock Eng 49(12):1–11. https://doi.org/10.1007/s00603-016-1079-9

Yao QL, Tang CJ, Sedighi M, Wang S, Huang QX (2019) Influence of moisture on crack propagation in coal and its failure modes. Eng Geol 258:105156. https://doi.org/10.1016/j.enggeo.2019.105156

Yilmaz I (2009) Influence of moisture content on the strength and deformability of gypsum. Int J Rock Mech Min 47(2):342–347. https://doi.org/10.1016/j.ijrmms.2009.09.002

Yin XT, Ge XR, Li CG, Wang SL (2010) Influences of loading rates on mechanical behaviors of rock materials. Chin J Rock Mech Eng 29(S1):2610–2615

Yu LQ, Yao QL, Li XH, Wang WN, Han H, Zhang MT (2020) Experimental study of failure characteristics and fissure propagation in hydrous siltstone. Arab J Geosci. https://doi.org/10.1007/s12517-020-05522-4

Yu LQ, Yao QL, Chong ZH, Li YH, Xu Q, Xie HX, Ye PY (2022) Mechanical and micro-structural damage mechanisms of coal samples treated with dry–wet cycles. Eng Geol 304:106637. https://doi.org/10.1016/j.enggeo.2022.106637

Zhang JX, Huang P, Zhang Q, Li M, Chen ZW (2017) Stability and control of room mining coal pillars-taking room mining coal pillars of solid backfill recovery as an example. J Cent South Univ 24(5):1121–1132. https://doi.org/10.1007/s11771-017-3515-8

Zhou ZL, Cai X, Cao WZ, Li XB, Cheng X (2016) Influence of moisture content on mechanical properties of rock in both saturation and drying processes. Rock Mech Rock Eng 49(8):3009–3025. https://doi.org/10.1007/s00603-016-0987-z